microbial biotechnology

Open Access

Brief Report

AntiV-SGN: a universal antiviral strategy to combat both RNA and DNA viruses by destroying their nucleic acids without sequence limitation

Kun Tian,[1,†] Zhen Qi,[1,2,†] Ying Chi,[3,†] Huanran Qiang,[1,†] Pei Wang,[1] Yu Liu,[1] Guohua Zhou,[4] Fengcai Zhu,[3,*] Qinglong Guo[1,] and Shu Xu[1,***]**

[1]*School of Basic Medical Science and Clinical Pharmacy, China Pharmaceutical University, Nanjing, 210009, China.*

[2]*Women's Hospital of Nanjing Medical University, Nanjing Maternity and Child Health Care Hospital, Nanjing, 210006, China.*

[3]*NHC Key Laboratory of Enteric Pathogenic Microbiology, Jiangsu Provincial Center for Disease Control and Prevention, Nanjing, 210009, China.*

[4]*Department of Pharmacology, Medical School, Jinling Hospital, Nanjing University, Nanjing, 210000, China*

.

Summary

Numerous viral outbreaks have threatened us throughout history. Here, we demonstrated a nucleic acid-based antiviral strategy named AntiV-SGN. Unlike those CRISPR-mediated methods, AntiV-SGN has advantages of no targets' sequence limitation, such as protospacer adjacent motif (PAM) or protospacer flanking sequence (PFS), being universal for both DNA and RNA viruses. AntiV-SGN was composed of a FEN1 protein and specific hpDNAs targeting viruses' nucleic acid. Its antiviral ability was tested on SARS-CoV-2 and HBV respectively. Reporter assays in human cells first illustrated the feasibility of AntiV-SGN. Then, it was verified that AntiV-SGN destroyed about 50% of live RNAs of SARS-CoV-2 in Vero cells and 90% cccDNA of HBV in HepG2.2.15 cells. It was also able to remove viral DNA integrated into the host's genome. In the mouse model, AntiV-SGN can be used to significantly reduce HBV expression at a level of 90%. Actually, in some cases, when viruses mutate to eliminate PAM/PFS or hosts were infected by both DNA and RNA viruses, AntiV-SGN could be a choice. Collectively, this study provided a proof-of-concept antiviral strategy of AntiV-SGN, which has potential clinical value for targeting a wide variety of human pathogens, both known and newly identified.

Introduction

Throughout the history of humanity, we have been threatened by numerous viral outbreaks, such as severe acute respiratory syndrome coronavirus 2 (SARS-CoV-2) (Huang *et al.*, 2020), Ebola (Rojek *et al.*, 2017) and AIDS (Margolis *et al.*, 2020). However, few vaccines or antivirals for known viruses have been approved (Freije and Sabeti, 2021). Traditional antivirals require knowledge of the optimal viral or host protein targets (De Clercq and Li, 2016) and rely on triggering the host immune response (Carrat and Flahault, 2007). We were even more unprepared for unknown viruses and lack of weapons for such kinds of sudden infectious diseases. Therefore, other technologies that only require knowledge of the genomic sequence of viruses could be critical for successfully responding to future outbreaks.

Recently, we developed and reported a hairpin DNA probe-SGN (HpSGN) system (Tian *et al.*, 2020). The HpSGN system is composed of the FEN1 nuclease and the hairpin DNA probe (designated hpDNA below). Moreover, the HpSGN system has been proved to

Received 14 December, 2021; revised 27 April, 2022; accepted 6 May, 2022.
For correspondence. *E-mail jszfc@vip.sina.com; Tel. +86-13951994867; Fax +86-025-86868499.
**E-mail anticancer_drug@163.com; Tel. +86-13801586679; Fax +86-025-83271055.
***E-mail rain_duly@163.com; Tel. +86-13951637529; Fax +86-025-83271055.
†These authors contributed equally to this work.
Microbial Biotechnology (2022) **15**(9), 2488–2501.

doi:10.1111/1751-7915.14076

Funding information

This work was supported by the National Natural Science Foundation of China (82 150 209, 32 071 440, 82 173 847). This work was supported by the Outstanding Young teacher sponsored by the Qing Lan Project in Jiangsu Province and the Postgraduate Research & Practice Innovation Program of Jiangsu Province (KYCX21_0661).

mediate genomic DNA modification and mRNA degradation (Tian *et al.*, 2020). The HpSGN system has advantages of (i) without sequence limitation like PAM or PFS; (ii) being able to cleave both DNA and RNA simultaneously; (iii) with smaller molecular weight and size (35 kDa, 337 amino acids) to delivery *in vivo* and *ex vivo*.

Therefore, we developed the HpSGN system as an antiviral strategy (designated AntiV-SGN strategy below) to break the viral genomic RNA of ssRNA viruses and viral genomic DNA of DNA viruses. For the ssRNA virus (a sample is SARS-CoV-2, Fig. 1), its spike protein unravels and pulls the membrane of the virus and host together, releasing the virus RNA genome into the cytoplasm. The virus transforms the cell's endoplasmic reticulum into bubble-like structures (called double-membrane vesicles, DMVs) which are proposed as cellular compartments for the viral RNA to replicate and transcribe (Snijder *et al.*, 2020). And then, newly synthesized genomes and subgenomic mRNAs (Hartenian *et al.*, 2020; V'Kovski *et al.*, 2021) will be released into the cytoplasm to package (Wolff *et al.*, 2020). The AntiV-SGN captures and degrades the genomic RNA and subgenomic mRNA in the cytoplasm to inhibit replication and viral gene expression. For the DNA viruses (a sample is HBV, Fig. 1), the virus infects cells and forms covalently closed circular DNA (cccDNA) (Ganem and Prince, 2004), which integrates into the host genomic

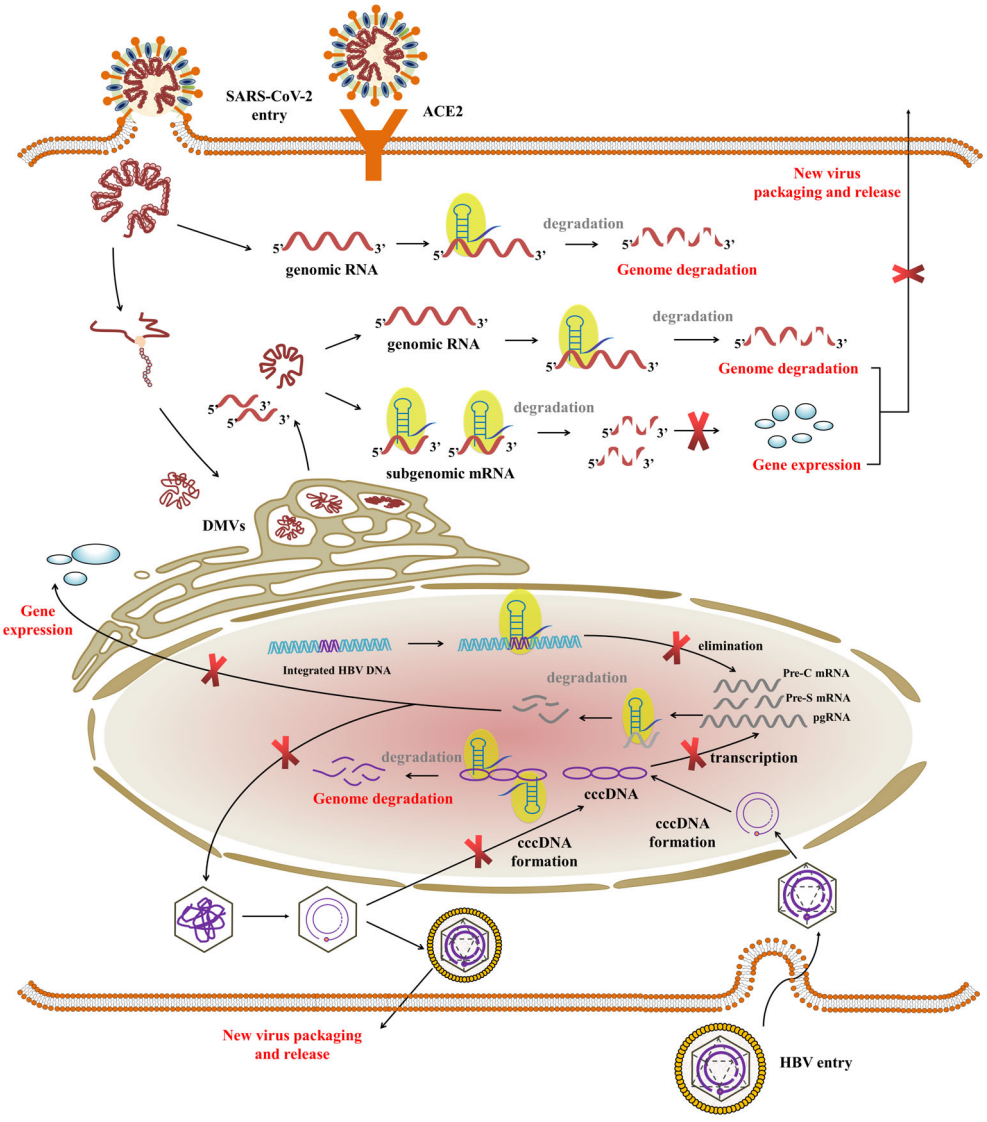

Fig. 1. Schematic of HBV/SARS-CoV-2 life cycle and putative antivirus effect of AntiV-SGN constructs. In the AntiV-SGN construct, the FEN1 was represented by a yellow ellipse, and the hpDNAs were represented by blue stem-loop lines.

DNA and makes lasting HBV infection (Block *et al*., 2007). The AntiV-SGN targets and destroys the cccDNA and viral fragment integrated into the host genomic DNA. Also, a recent study reported evidence that the SARS-CoV-2 subgenomic RNAs can be reverse transcribed and integrated into the host's genomic DNA by cellular reverse transcriptase (long interspersed element-1, LINE1) (Zhang *et al*., 2021). Therefore, directly attacking the genetic materials (both DNA and RNA), which are the fundamental keys of viruses, may be done once and for all in antiviral treatments.

Although the CRISPR-Cas9 system has been successfully applied to directly disrupt essential genes of both DNA viruses and RNA viruses (Price *et al*., 2015; Li *et al*., 2016; Roehm *et al*., 2016; Bella *et al*., 2018), the CRISPR-Cas13 system was used to reduce levels of viral RNA (Abbott *et al*., 2020; Blanchard *et al*., 2021). However, it is wondering whether there is another nucleic acid-based antiviral capable of combating not only DNA viruses but also ssRNA viruses. In addition, we are worried that viruses may mutate and eliminate the PAM/PFS to escape the attack from CRISPR-mediated antivirals because the PAM (Wang *et al*., 2015; Hu *et al*., 2018) or PFS (Abudayyeh *et al*., 2017; Cox *et al*., 2017) is necessary for Cas9 or Cas13 nuclease respectively.

The feasibility of the constructed AntiV-SGN strategy will be tested *ex vivo* and *in vivo* in this study. We hypothesized that this proof-of-concept antiviral strategy of AntiV-SGN has potential clinical value for targeting a wide variety of human pathogens, both known and newly identified.

Results

AntiV-SGN is capable of inhibiting SARS-CoV-2 reporter expression in human cells

SARS-CoV-2 has an ssRNA genome with 30 000-nt encodes 12 functional open reading frames (Chan *et al*., 2020). A previous study (Abbott *et al*., 2020) reported highly conserved regions to contain the nucleocapsid (N) gene at the end of the genome, which encodes the capsid protein for viral packaging. Since our HpSGN system has no limitation of targets' sequence (like PAM/PFS), theoretically, any position in the *N* gene could be the candidate location of hpDNAs. However, guide sequences potentially binding in the human reference genome should be excluded. Then, four hpDNAs (shorted as Hp-1, Hp-2, Hp-3 and Hp-4) targeting the *N* gene were designed and synthesized (Fig. 2A, Table S1).

To verify the feasibility of the AntiV-SGN strategy in human cells, we synthesized a gene encoding the *A. fulgidus* FEN1 gene (1011 bp, 337 amino acids, 35 kDa) and attached a C-terminal NES for optimal expression in the cytoplasm. Then, sequence coding of the N protein of SARS-CoV-2 was inserted into the reading frame of EGFP protein to construct a reporter plasmid (Table S2). Those two plasmids and hpDNAs were transfected into A549 cells, followed by detection of the EGFP reporter expression level and CoV-N fragment mRNA transcript abundance (Fig. 2B). As shown in Fig. 2C, relative to the group transfected with non-targeting hpDNAs, the groups transfected with Hp-1, Hp-2, Hp-3 and Hp-4 downregulated the EGFP reporter expression by 52%, 54%, 51% and 45%. The percentages of EGFP positive cells decreased from 25.5% (non-targeting group) to 8.18%, 8.24%, 8.72% and 10.8% in Hp-1, Hp-2, Hp-3 and Hp-4 groups respectively (Fig. 2D). Following this, one pool of targeting hpDNAs (Hp-1, Hp-2, Hp-3 and Hp-4 mixture) was used to repress the CoV-N fragment mRNA transcript abundance, causing a ~ 39% inhibition (Fig. 2E, Table S4). Given that the processes of both degradation of transcripts and post-translational modification affect the uniformity of mRNA and protein, the transcription level and translation level are not completely consistent.

Then, we also constructed another reporter plasmid, which contained a fragment encoding the *RdRP* gene (Table S2). Then, four hpDNAs targeting the *RdRP* gene (shorted as Hp-R1, Hp-R2, Hp-R3 and Hp-R4, the detailed sequence is shown in Table S1), excluding potential mismatch in the human genome, were designed and synthesized. We co-transfected the EGFP reporter and AntiV-SGN into human cells. After being treated by AntiV-SGN, the efficiency of a downregulation for EGFP mRNA was detected by qPCR analysis. As shown in Fig. S1, relative to the group transfected with non-targeting hpDNAs, the groups transfected with Hp-R1, Hp-R2, Hp-R3 and Hp-R4 repressed the EGFP reporter by 64%, 80%, 77% and 23% of RNA abundance in HEK293T cells respectively.

Next, we compared the strategies of AntiV-SGN, RNAi and CRISPR-Cas13 in HEK293A, A549 and HepG2 cells with three identical random targeting loci (T1, T2 and T3) (Fig. 2F). For each locus, targeting hpDNA, siRNA and crRNA were designed with the same guide sequence (Tables S1 and S3). AntiV-SGN performed better than the other two strategies at the T2 locus in A549 cell (24.4% inhibition) and T2/T3 loci in HepG2 cells (23.7% and 49.2% inhibition respectively). Meanwhile, Cas13 had outstanding behaviour at the T1 locus in HEK293A cell (89.9% inhibition), T3 locus in HepG2 cell (49.2% inhibition) and T1/T3 loci in A549 cells (23.0% and 37.0% inhibition respectively). Moreover, RNAi stood head at T2/T3 locus in HEK293A cell (31.6% and 20.3% inhibition respectively). In addition, we found that the AntiV-SGN (NLS-FEN1) and CRISPR (Cas9) induced cell viability inhibition in HEK293T and A549 cells. Cell death was also observed in A549 cells treated by AntiV-SGN (FEN1-NES) and CRISPR (Cas13) (Fig. S2). The knocking-down

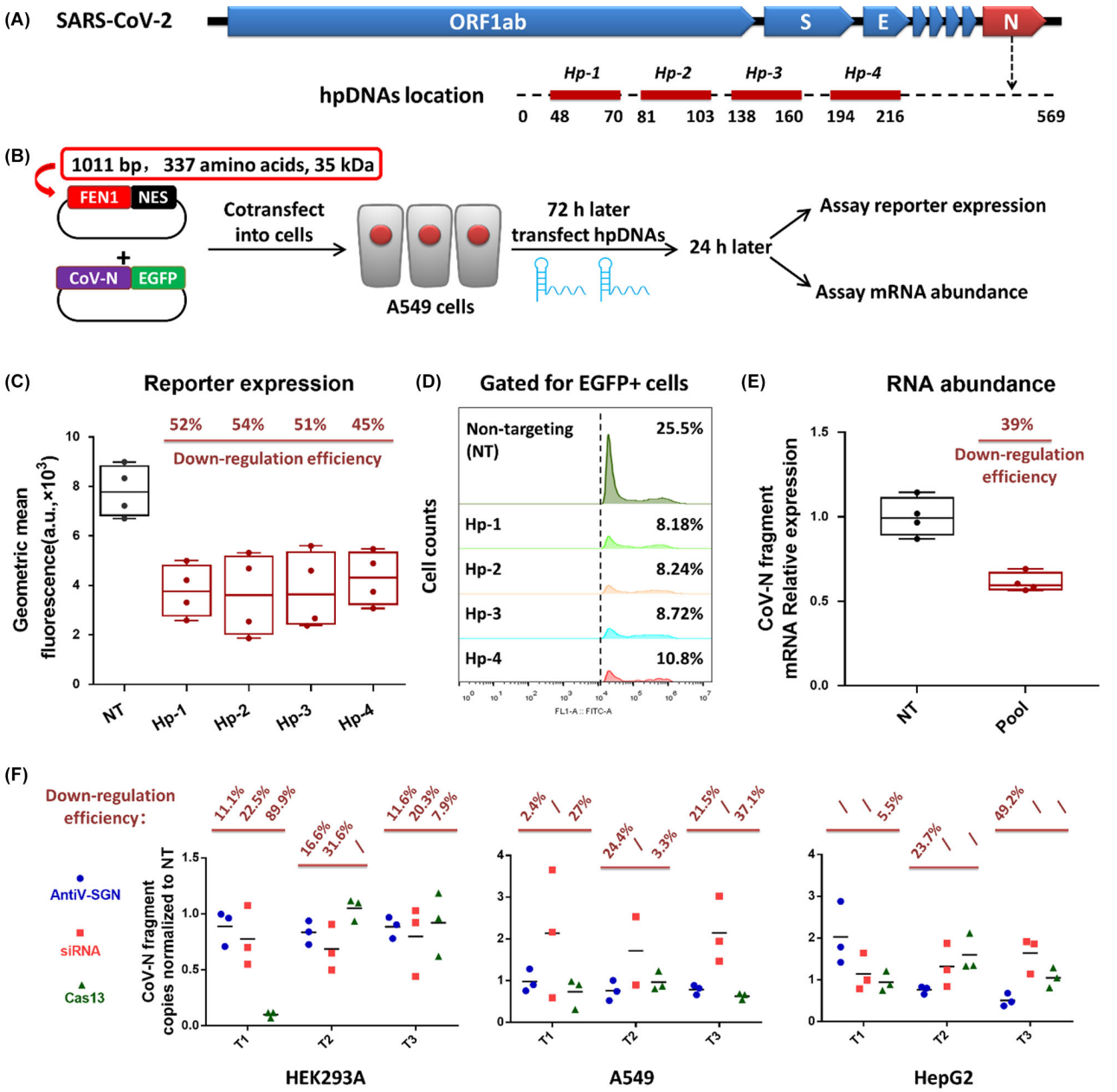

Fig. 2. AntiV-SGN is capable of inhibiting SARS-CoV-2 reporters' expression in human cells.
A. The locations of hpDNAs targeting the *N* gene of SARS-CoV-2.
B. Experiment workflow to challenge AntiV-SGN in A549 lung epithelial cells with CoV-N reporters.
C. The EGFP reporter expression of groups transfected with non-targeting hpDNA (NT) and targeting hpDNAs (Hp-1, Hp-2, Hp-3 and Hp-4). $n = 4$, two-tailed Student's *t*-test; *P* values for Hp-1 ($P = 0.0016$), Hp-2 ($P = 0.005$), Hp-3 ($P = 0.005$) and Hp-4 ($P = 0.0034$) are relative to NT.
D. Representative flow histograms of EGFP reporter levels after treated by AntiV-SGN. Cells shown were gated for EGFP+ cells only.
E. The CoV-N fragment mRNA relative expression of groups transfected with non-targeting hpDNA (NT) and one pool of targeting hpDNAs (Hp-1, Hp-2, Hp-3 and Hp-4 mixture). $n = 4$, two-tailed Student's *t*-test; $P = 8 \times 10^{-4}$.
F. Comparison of AntiV-SGN, siRNA and Cas13 strategy to cleaving RNA fragments from SARS-CoV-2 sequences in HEK293A, A549 and HepG2 cells. $n = 3$.

ability variation was likely due to cell line characteristics, antivirus strategies' delivery efficiency and cell toxicity. It reminds us that the robust performance of the nucleic acid-based antiviral strategy may be inseparable from effective delivery and good biosafety. For the AntiV-SGN strategy, the small size of FEN1 protein (337 amino acids) and no sequence limitation of targets seem to be beneficial in some situations. The results indicated that AntiV-

SGN could be an alternative complementary option for the other two classical methods (RNAi and CRISPR-Cas13).

AntiV-SGN has potent antiviral activity against SARS-CoV-2 in Vero cells

We tried to evaluate AntiV-SGN's potential to serve as a programmable antiviral platform to combat a representative of ssRNA viruses, SARS-CoV-2. The FEN1-NES plasmid was transfected into Vero cells for 48 h. Then, the cells were inoculated by SARS-CoV-2, and a pool of hpDNAs (Table S1, as same as hpDNAs used in Fig. 2E) was transfected 24 h later. The viral RNA (vRNA) from the cell supernatant was collected to perform absolute quantitative real-time PCR to examine the vRNA level (Fig. 3A, Table S4). The effects of AntiV-SGN against SARS-CoV-2 at MOIs of 0.008 and 0.16 levels in Vero cells were tested. With an MOI of 0.008, a 60% ($P = 0.0079$) reduction in vRNA compared with the targeting group and virus-only group was measured by RT-qPCR 48 h post infection (hpi) (Fig. 3B). A 44% ($P = 0.0246$) reduction in vRNA compared with the targeting group and non-targeting group was measured. With MOI of 0.16, the 42% ($P = 0.0099$) and 39% ($P = 0.1299$) reduction relative to virus-only group and non-targeting group were observed (Fig. 3B). It indicated that the AntiV-SGN could destroy about 50% of live vRNAs of SARS-CoV-2 in Vero cells within 24 h. However, after being treated by AntiV-SGN, we did not inspect an obvious recovery of the cellular state of the SARS-CoV-2 infected cells. Compared with the CRISPR-based anti-SARS-CoV-2 strategy (Blanchard *et al.*, 2021), which has a great effect on increasing the percentage of live cells, the CRISPR-based strategy can reduce several orders of magnitude the *RdRP* or *N* gene copy number. This result indicated that the current AntiV-SGN is not robust enough to give sufficient clinical benefits and needs further improvement.

Besides, known viral DNA and RNA are actively evolving *in vivo*, which leads to mutations in their coding sequence to escape from nucleic acid-based antivirals. Target site mutations can reduce the potency of many antiviral approaches, and thus, the propensity for these mutations to rise following treatment should be monitored. To answer whether the unsolved SARS-CoV-2 in cell supernatant varied their sequences to escape being recognized by our AntiV-SGN or not (within the experimental time period, 4 days), the vRNA collected from the remaining SARS-CoV-2 was sequenced. The results in Fig. 3C showed that no virus was mutant, which indicated that AntiV-SGN did not force the virus to change the sequence for absconding. Future work will be required to evaluate the timescale and the degree to which viral RNAs can evolve resistance to AntiV-SGN targeting.

AntiV-SGN is capable of inhibiting HBV fragment expression in human cells

To verify the feasibility of the AntiV-SGN strategy against DNA virus, the sequence coding the X protein of Hepatitis B Virus (HBV) was inserted into the reading frame of EGFP protein, and three pairs of hpDNAs targeting X ORFs were designed (Fig. 4A, Hp-1 pairs, Hp-2 pairs and Hp-3 pairs), excluding potential mismatch in the human genome.

To evaluate the efficacy, we co-transfected the HepG2 cells with the HBV-X reporter plasmid, the NLS-FEN1 coding plasmid and individual hpDNAs pairs, followed by detection of the EGFP reporter expression level and HBV-X fragment mRNA transcript abundance (Fig. 4B). As shown in Fig. 4C, relative to the group transfected with non-targeting hpDNAs, the groups transfected with Hp-1 pairs, Hp-2 pairs and Hp-3 pairs downregulated the EGFP reporter expression by 43%, 56% and 66% respectively. Moreover, as shown in Fig. 4D, these hpDNA pairs decreased the HBV-X fragment mRNA transcript abundance levels by 36%, 27% and 29% respectively.

Next, we compared the strategies of AntiV-SGN, RNAi and CRISPR-Cas9 at an identical random targeting locus (Fig. 4E). The targeting hpDNA, siRNA and sgRNA were designed with the same guide sequence (Tables S1 and S3). CRISPR-Cas9 performed effectively and inhibited the HBV-X fragment mRNA about 37% and 61% in HEK293A and HepG2 cells respectively. In parallel, AntiV-SGN had efficiencies of 28% and 39% knockdown at this locus respectively. Compared to AntiV-SGN, RNAi strategy was adversely affected in HepG2 cells. The results indicated that AntiV-SGN could be an alternative complementary option for the other two classical methods (RNAi and CRISPR-Cas9).

AntiV-SGN has potent antiviral activity against HBV in human cells

To evaluate the ability of DNA viruses' clearance mediated by AntiV-SGN, the NLS-FEN1 coding plasmid with a pool of hpDNAs was transfected into HepG2.2.15 cell (Sells *et al.*, 1987), which has four 5′-3′ tandem copies of HBV genome and is an ideal model for investigating HBV (Ramanan *et al.*, 2015) (Fig. 5A). Target loci of hpDNAs were chosen to maximize conservation across

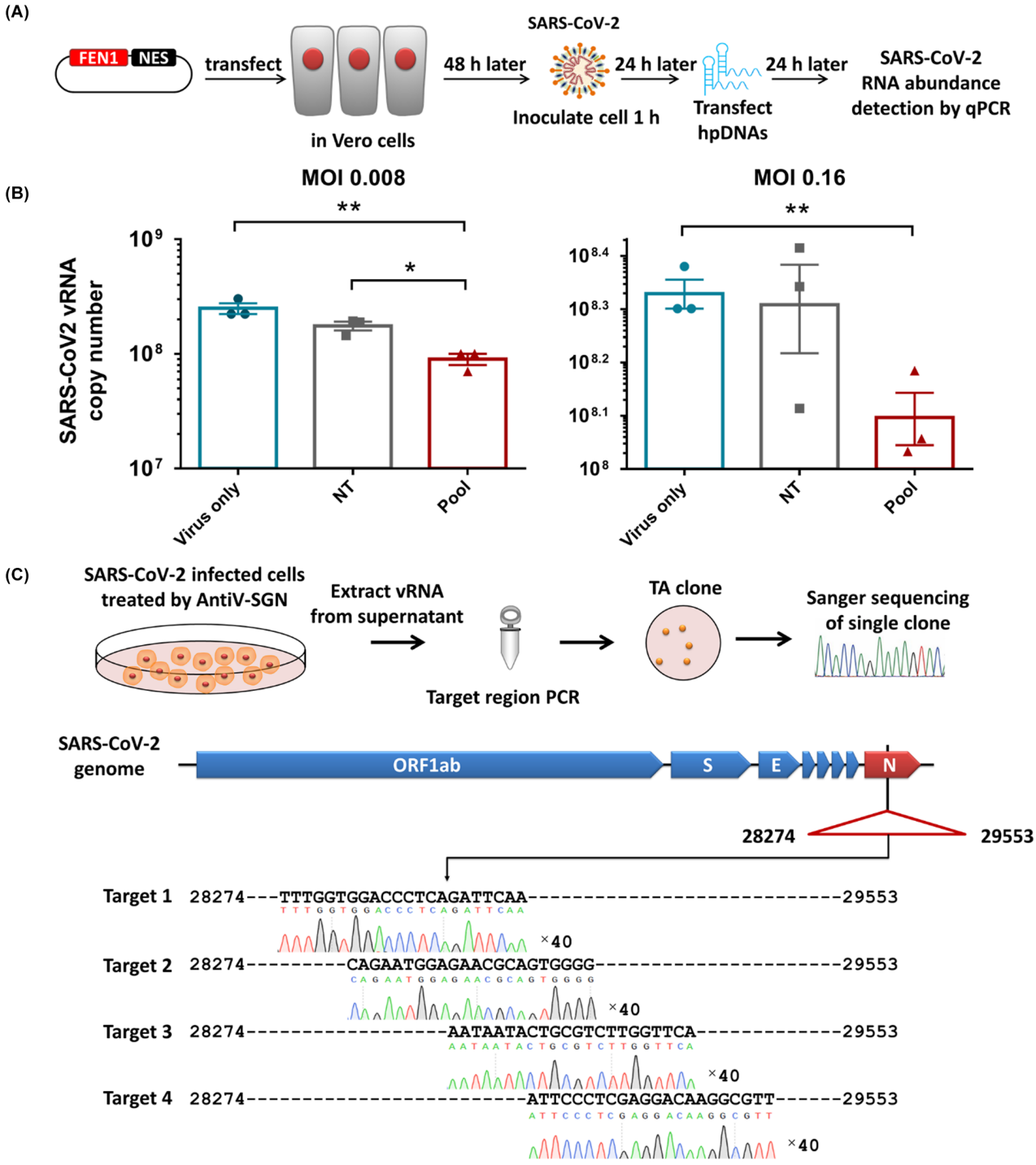

Fig. 3. AntiV-SGN has potent antiviral activity against SARS-CoV-2 in Vero cells.
A. Experiment workflow to challenge AntiV-SGN in Vero cells infected with SARS-CoV-2.
B. Copy number of SARS-CoV-2 vRNA levels 24 hpi when transfection of FEN1-NES and targeting hpDNAs or non-targeting hpDNAs (NT) and virus only group. $n = 3$, two-tailed Student's *t*-test; *, $P = 0.009$ and **, $P = 0.0048$ for MOI = 0.008; **, $P = 0.01$ for MOI = 0.16; bars represent mean ± SEM.
C. Sequences of the vRNA collected from remaining SARS-CoV-2. Forty clones were collected to be sequenced.

viral genotypes and minimize homology to the human genome (Fig. 5B). Based on these criteria, we designed three pairs of hpDNAs (Hp-1 pairs, Hp-2 pairs and Hp-3 pairs, Table S1). The cccDNA in the nucleus was extracted and quantified by qPCR (detail in the Method section, Table S4). As shown in Fig. 5C, quantitative

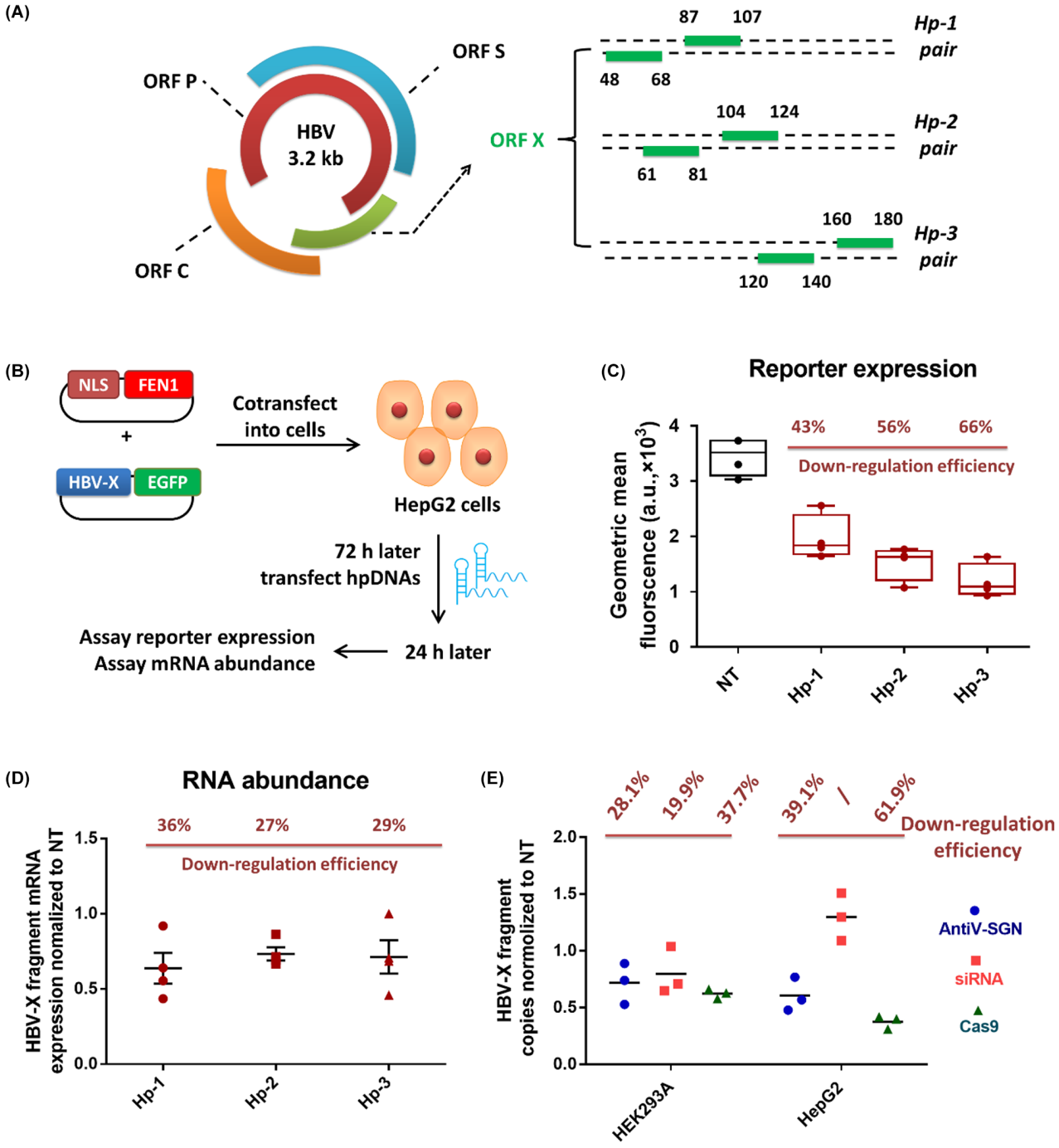

Fig. 4. AntiV-SGN is capable of inhibiting HBV fragment expression in human cells.
A. The locations of hpDNA pairs targeting X ORFs of HBV.
B. Experiment workflow to challenge AntiV-SGN in HepG2 cells with HBV-X reporters.
C. The EGFP reporter expression of groups transfected with non-targeting hpDNA (NT) and targeting hpDNA pairs (Hp-1, Hp-2 and Hp-3). $n = 3$, two-tailed Student's *t*-test; *P* values for Hp-1 ($P = 0.0014$), Hp-2 ($P = 0.00017$) and Hp-3 ($P = 6.7 \times 10–5$) are relative to NT.
D. The HBV-X fragment mRNA relative expression of groups transfected with non-targeting hpDNA (NT) and targeting hpDNAs pairs. $n = 3$ or 4; bars represent mean ± SEM.
E. Comparison of AntiV-SGN, siRNA and Cas9 strategy to cleaving RNA fragments from HBV-X sequences in HEK293A and HepG2 cells. $n = 3$.

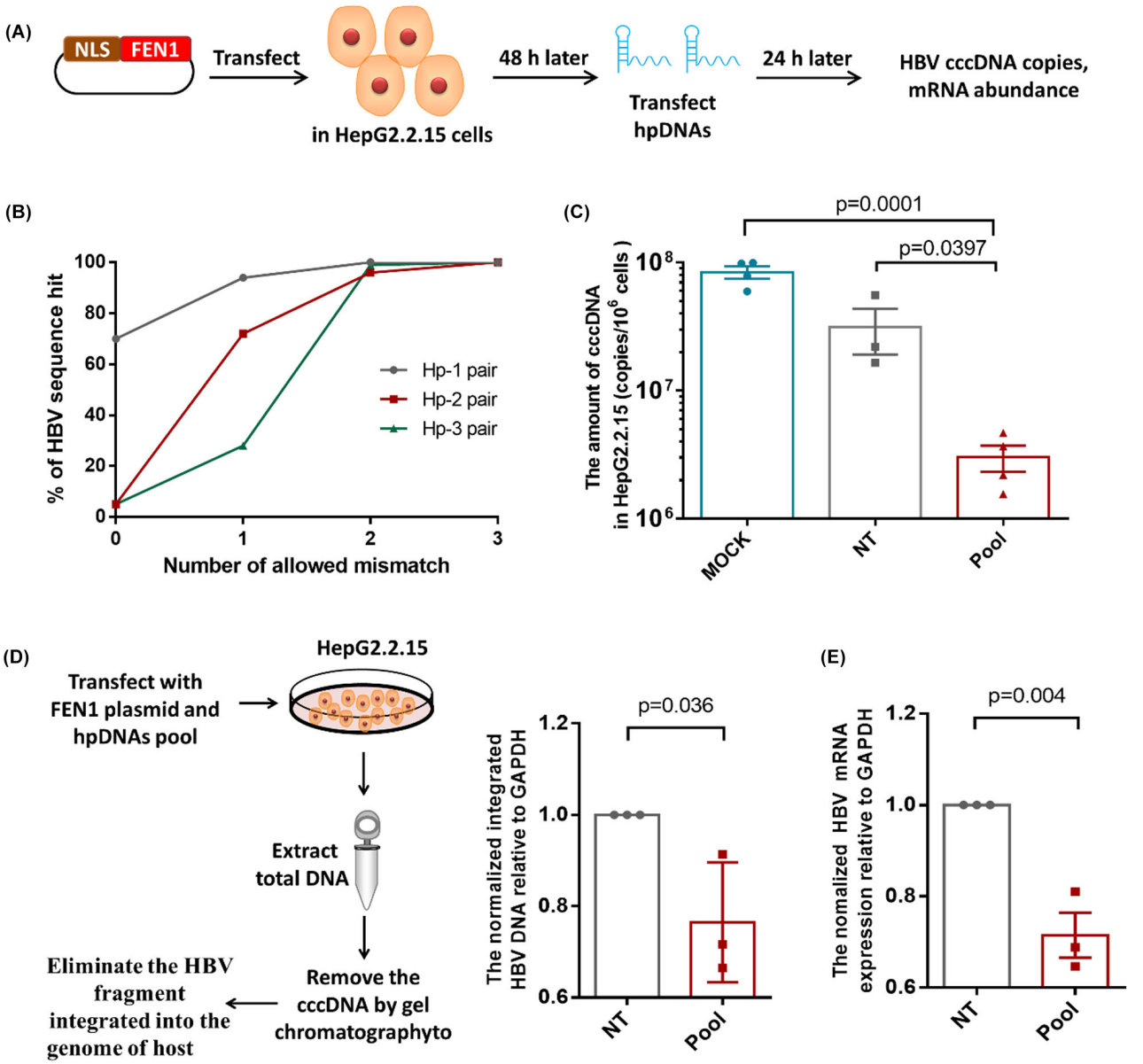

Fig. 5. AntiV-SGN has potent antiviral activity against HBV in human cells.
A. Experiment workflow to challenge AntiV-SGN in HepG2.2.15 cells.
B. 100 HBV isolates were chosen from GenBank to testify the coverage of hpDNAs. The *x*-axis denotes the number of allowed mismatches, and the *y*-axis denotes the percentage of sequenced isolates that fall within this number of mismatches to the native hpDNA target site.
C. The cccDNA levels of the mock group transfected with non-targeting hpDNA (NT) and targeting hpDNA pairs. $n = 3$ and $n = 4$, two-tailed Student's t-test; *P* values for pool ($P = 0.0001$) are relative for MOCK (HepG2.2.15 without transfected any plasmids), *P* values for pool ($P = 0.0397$) are relative for NT; bars represent mean ± SEM.
D. The HBV fragment integrated into the genome of HepG2.2.15 levels of transfected with non-targeting hpDNA (NT) and targeting hpDNA pairs. $n = 3$, two-tailed Student's t-test; *P* values for pool ($P = 0.036$) are relative for NT; bars represent mean ± SEM.
E. The HBV mRNA expression levels of transfected with non-targeting hpDNA (NT) and targeting hpDNA pairs. $n = 3$, two-tailed Student's *t*-test; *P* values for pool ($P = 0.004$) are relative for NT; bars represent mean ± SEM.

PCR showed a robust 90.4% ($P = 0.0397$) reduction in cccDNA compared with control groups transfected with FEN1 coding plasmid plus non-targeting hpDNAs. Moreover, a higher reduction (96.4%, $P = 0.0001$) compared with control groups without FEN1 and hpDNAs.

Then, to answer whether the AntiV-SGN could be used to clean the HBV fragment integrated into the genome of the host, the total DNA was isolated from AntiV-SGN treated HepG2.2.15, and we removed the cccDNA by gel chromatography to get the genomic DNA (Fig. S3). As shown

in Fig. 5D, the AntiV-SGN could eliminate about 25% of integrated HBV DNA in HepG2.2.15. In our previous study, we demonstrated that FEN1 driven prefers inducing large fragment mutations on targeting locus; therefore, the FEN1 has a higher probability in the ability to eliminate integration compared to Cas9-driven mutagenesis. These results were confirmed by reducing HBV mRNA (~ 29%) to controls transfected with FEN1 coding plasmid plus non-targeting hpDNAs (Fig. 5E), which was possibly an additive effect of the combination of DNA cleaving and mRNA cleaving. These results demonstrate that targeting multiple conserved regions of HBV with AntiV-SGN could result in suppression of viral transcription, depletion of cccDNA and elimination of integrated HBV DNA.

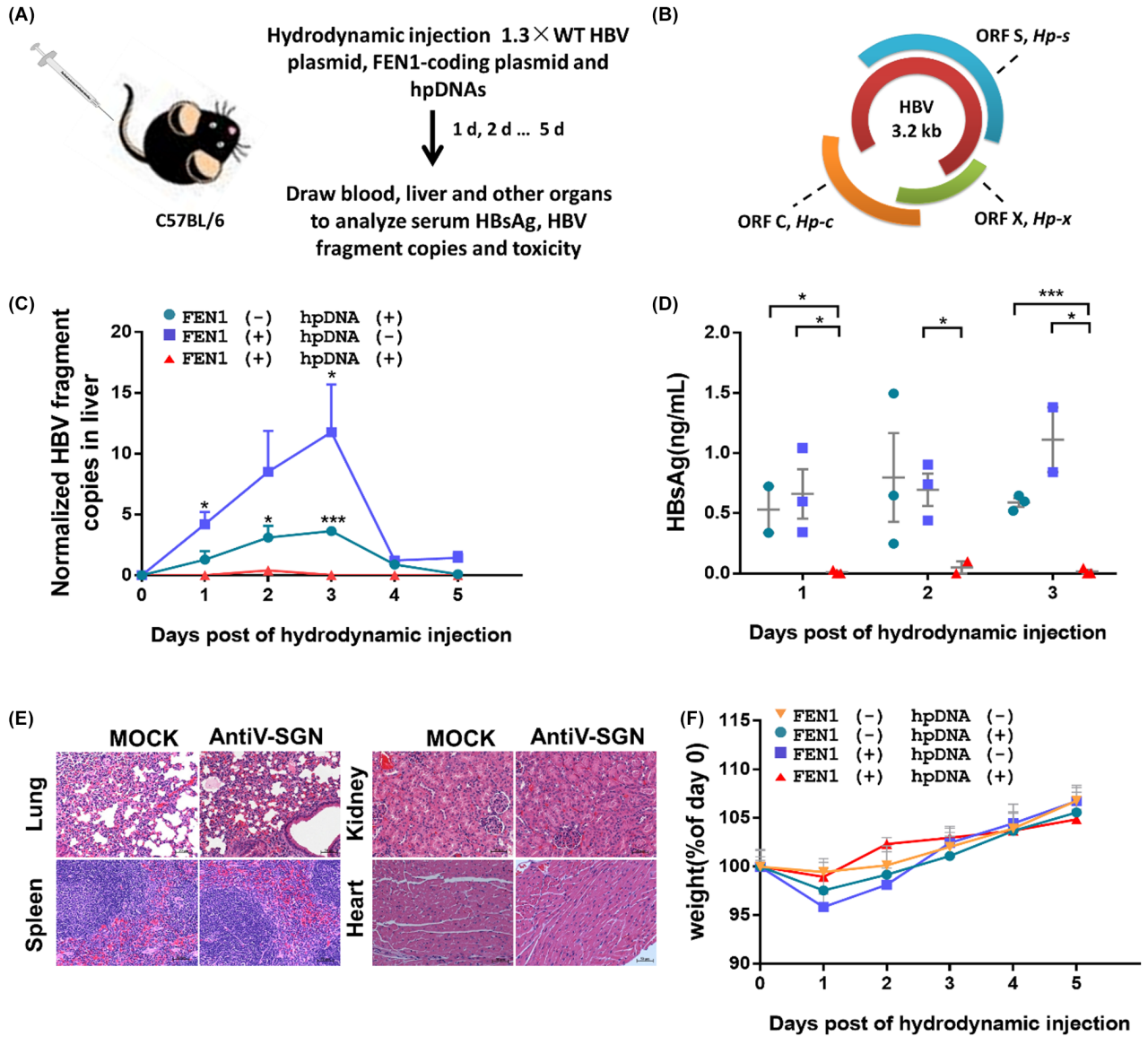

Fig. 6. Confirmation of anti-HBV effect *in vivo*.
A. Experimental schematic for: 1.3 × WT HBV, FEN1-coding plasmid and hpDNAs are delivered to the livers of C57BL/6 mice via hydrodynamic injection.
B. The locations of hpDNA pairs targeting 1.3 × WT HBV.
C. HBV mRNAs are quantified in mouse liver at indicated time point post injection. All the points were normalized to the C57BL/6 which was treated with EV plasmid and targeting pool. n = 3, two-tailed Student's *t*-test; *, $P < 0.05$; ***, $P < 0.001$; bars represent mean ± SEM.
D. HBsAg are quantified in mouse blood at indicated time point post injection. $n = 2$ or n = 3, two-tail Student's *t*-test; *, $P < 0.05$; ***, $P < 0.001$; bars represent mean ± SEM.
E. Representative haematoxylin and eosin (H&E) of C57BL/6 mice injected control and FEN1-expressing plasmid at the 5th day. Scale bars are 50 mm. MOCK: The C57BL/6 did not treat with any plasmids.
F. Bodyweight changes of mice during 5 days post infection. Mice were injected with 1.3 × WT HBV. $n = 4$, bars represent mean ± SEM.

Confirmation of anti-HBV effect in vivo

To testify that our AntiV-SGN functioned appropriately in primary hepatocytes, we sought to evaluate the antiviral effect of AntiV-SGN for HBV *in vivo*. HBV plasmid, FEN1 plasmids and hpDNAs were introduced to the liver of C57BL/6 mouse by hydrodynamic injection (HDI) (Fig. 6A). The HBV genome ORF and location of target sequences for hpDNAs are shown in Fig. 6B (Table S1). Animals expressing FEN1 and hpDNAs in this model showed a progressive suppression of HBV expression compared to controls, reflected by a 90% decrease in HBV mRNA expression level on days 2 and 3 post injection (Fig. 6C). Corresponding to the efficiency in the liver, the level of HBsAg serum rapidly decreased and even became undetectable at the indicated time point (Fig. 6D).

What is more, we testified whether the expression of FEN1 causes an adverse effect in C57BL/6 mice or not; we collected the lung, kidney, spleen and heart of the mice treated by AntiV-SGN. As shown in Fig. 6E, the expression of FEN1 did not cause obvious cytotoxicity on mice's organ cells. Meanwhile, FEN1 led to no significant reduction in body weight (Fig. 6F). Collectively, these findings verified that AntiV-SGN possessed a strong antiviral effect *in vivo* in parallel with low toxicity. Therefore, it has the potential to be developed as an ideal candidate for virus treatment.

Discussion

Here, we demonstrated a nucleic acid-based antiviral strategy named AntiV-SGN. We first proved that the AntiV-SGN can effectively target and cleave EGFP reporter plasmids of CoV-N protein and HBV-X protein by both RNA abundance and reporter expression detection. In comparison with the other two kinds of nucleic acid-based methods (RNAi and CRISPR system), our AntiV-SGN performed similarly. Next, AntiV-SGN was illustrated with antiviral activity against SARS-CoV-2 in Vero cells and HBV in HepG2.2.15 cells and C57BL/6 mice. We demonstrated the ability to cleave vRNA, cccDNA, integrated vDNA and other viral gene expression and replication parameters by the AntiV-SGN strategy.

One of the potential advantages of AntiV-SGN is its size. A nucleic acid-based antiviral used in the clinic has to be delivered effectively and safely *in vivo*. One attractive choice being employed is to deliver a ribonucleoprotein complex containing the FEN1 protein assembled with hpDNAs. In the CRISPR-associated system, several works have proven the feasibility of this ribonucleoprotein complex strategy (Staahl *et al*., 2017). In the AntiV-SGN system, the FEN1 protein has only 337 amino acids, much smaller than the Cas-family protein. Besides, the synthesis of a DNA probe with a length of ~ 50 nt is easier and cheaper than an RNA probe. Another attractive choice is the liposomal delivery strategy, in which nuclease could be delivered in mRNA form within chemical polymers or lipid nanoparticles (LNPs). In a CRISPR-associated system, the length of mRNA of Cas-family protein could be several thousands of bases and complicated to the transcript *in vitro* by transcription kits. Instead, the mRNA of FEN1 protein is much shorter, which is only ~ 1000 nt bases.

Another potential advantage of AntiV-SGN is its resulting form, which introduces large fragment deletions, not small indels (short for insertion and deletion) on the virus coding sequence. In some cases, small indels disrupted by Cas-family protein are still translated into effective proteins and lead to escape mutations. Large fragments deletions (> 100-nt) on the virus coding sequence will destroy several ORFs and functional domains of proteins.

Currently, in this study, not all of hpDNAs work well. Delivery of multiple hpDNAs with more binding sites is also effective. Fortunately, the large fragment deletions made by AntiV-SGN weaken the need to test a large number of hpDNAs sequences to identify ones with potency. But the second structure of oligonucleotide assembly and the locations of nucleic acid-based antiviral on different functional domains in viruses may also affect the cleaving results. Further research is required to accelerate progress towards an antivirus therapeutic. Beyond antiviral value, the AntiV-SGN may also potentially be used as a research tool to investigate viral evolution because we found that FEN1 can capture but not cleave DNA/ RNA targets (submitted elsewhere).

Moreover, one of the disadvantages of AntiV-SGN is its relatively weak efficiency. In our opinion, changing hpDNA probes into hpRNA probes may be helpful to improve efficiency. Because the amount of hpRNA probes being transcripted is more than that of hpDNA probes. The other disadvantage of AntiV-SGN is the worry about its safety (including the off-target issue). In the future, we try to synthesize *in vitro* transcribed mRNA (Loomis *et al*., 2018; Tiwari *et al*., 2018) to express FEN1 or deliver a ribonucleoprotein complex (Xu *et al*., 2021) containing the FEN1 protein assembled with hpDNAs to reduce the time span of FEN1 in human cells. We anticipate that one of the above-mentioned strategies can potentially contribute to the AntiV-SGN's practical antiviral application beyond only a proof-of-principle method.

Whilst we sought to bioinformatically predict this potential off-target activity of cellular transcripts by aligning the hpDNAs to the human genome, however, this bioinformatic prediction of off-target activity requires

further validation experimentally using transcriptome analysis and genome analysis. In the future, we try to minimize the off-targeting using the following methods in the future study: i) optimizing the length of or modifying the hpDNAs; ii) choosing an optimal delivery form of AntiV-SGN to reduce the time span of FEN1 expression; iii) adding a switch to regulate the activity of AntiV-SGN.

In summary, this study provided a proof-of-concept antiviral strategy of AntiV-SGN to combat both DNA and RNA virus, which has potential clinical value for targeting a wide variety of human pathogens, both known and newly identified.

Experimental procedures

Construction of plasmid expressing FEN1

The plasmids were constructed as described before (Tian *et al*., 2020). For HBV relative experiments, NLS was added to the N-terminus of *A. fulgidus* and then subcloned to pcDNA3.1(+) to generate pcDNA3.1(+)-HA-NLS-*A. fulgidus* FEN1. For SARS-CoV-2 relative experiments, NLS was substituted by NES to generate pcDNA3.1(+)-HA-*A. fulgidus* FEN1-NES.

Design and cloning of CoV-N/CoV-RdRP/HBV-X reporter

The sequence coding the N protein or RdRP protein of SARS-CoV-2 and X protein of HBV was inserted into the reading frame of EGFP protein to form a CoV-N/CoV-RdRP/HBV-X reporter plasmid. The pEGFP-N1 vector was digested with *HindIII* and *KpnI*. The fragments CoV-N or CoV-RdRP and HBV-X were synthesized by the GenScript biotechnology company. Last, the fragments inserted the pEGFP-N1 vector using T4 DNA Ligase (Vazyme, C301-01, Nanjing, China) (the detailed sequences are shown in Table S2).

Cell culture

HEK293T, Vero, HepG2, A549 and HepG2.2.15 cells were maintained in Dulbecco's modified Eagle's Medium (DMEM) or RPMI-1640 supplemented with 10% fetal bovine serum (HyClone, Logan, UT, USA), 100 U ml^{-1} of penicillin and 100 μg ml^{-1} of streptomycin at 37°C with 5% CO_2 incubation.

CoV-N/CoV-RdRP/HBV-X reporter test

On day 1, cells were seeded into 24-well plates (Corning, Corning, NY, USA) at a density of 70 000 cells per well. On day 2, cells were transfected with CoV-N/CoV-RdRP/HBV-X reporter plasmid (0.1 μg per well) and pcDNA3.1(+)-HA-*A. fulgidus* FEN1-NES (in CoV-N reporter test)/ pcDNA3.1(+)-HA-NLS-*A. fulgidus* FEN1 (in HBV-X reporter test) (0.5 μg per well). Then, 60–72 h later, cells were transfected with hpDNAs (600 pmoL per well) (the detailed sequences are shown in Table S1). Twenty-four hours after transfection of hpDNAs, cells were harvested and tested using flow cytometry to detect EGFP reporter expression and using relative quantitative PCR to detect CoV-N/CoV-RdRP/HBV-X fragment mRNA abundance. For RNAi and CRISPR groups, 50 pmoL siRNA or 1 μg plasmid expressing Cas13a-sgRNA (in CoV-N reporter test)/Cas9-sgRNA (in HBV-X reporter test) were used (the detailed sequences are shown in Table S2).

Flow cytometric analysis

The cells were resuspended in PBS; the fluorescence intensity (EGFP 488 nm excitation and 525 nm emission) was measured immediately using BD Accuri™ C6 Plus. 10 000 cells were counted and measured in each sample. The EGFP fluorescence was calculated by subtracting the geometric mean EGFP fluorescence measured in mock-infected samples. Each sample was measured four times and got an average value.

$$\text{Efficiency}\,(\%) = \frac{(\text{Fb-Fa})\text{-}(\text{Fc-Fa})}{\text{Fb-Fa}} = \frac{(\text{Fb-Fc})}{\text{Fb-Fa}},$$

Fa, the fluorescence intensity of the wild-type cells; Fb, the fluorescence intensity of the cells transfected with FEN1 and reporter plasmid; Fc, the fluorescence intensity of the cells transfected with FEN1, reporter plasmid and hpDNA

Relative quantitative PCR

Cells were trypsinized and washed once with PBS, and total RNA was isolated with RNA-easy Isolation Reagent (Vazyme, R701-01/02) following the manufacturer's instructions. For mRNA, cDNA synthesis was performed using the HiScript III 1st Strand cDNA Synthesis Kit (+gDNA wiper) (Vazyme, R312-01). The cDNA was used in quantitative PCR analyses with AceQ qPCR SYBR Green Master Mix (Low ROX Premixed) (Vazyme, Q131-02) with specific primers listed in Table S4. Relative gene expression was calculated using the ΔΔCt method. Results were normalized to *Gapdh*.

CCK8 assay

On day 1, cells were seeded into 96-well plates (Corning) at a density of 8000 cells per well. On day 2, cells were transfected with CoV-N reporter plasmid (0.02 μg per well), pcDNA3.1(+)-HA-*A. fulgidus* FEN1-NES (0.08 μg per well) and Cas13a-NES (0.08 μg per well) (in CoV-N reporter test); cells were transfected with HBV-X reporter

plasmid (0.02 μg per well), pcDNA3.1(+)-HA-NLS-*A. fulgidus* FEN1 (0.08 μg per well) and Cas9-NLS (0.08 μg per well) (in HBV-X reporter test). Then, 24 h later, cells were transfected with hpDNAs (50 pmoL per well) and sgRNA plasmid (0.08 μg per well). Twenty-four hours after transfection of hpDNAs and sgRNA, 10 μl of CCK8 solution was added to each well and incubated for 4 h at 37°C. Absorbance was read at 450 nm with a Synergy™ HT multi-mode reader (Bio-Tek, Winooski, VT, USA). The average value of the optical density (OD) of five wells was used to determine cell viability according to the following formula: Inhibition rates (%) = (1 − OD treatment group/OD control group) × 100%.

Off-target mapping

To characterize the specificity of hpDNAs, we ensured that hpDNA does not target any sequences in the human reference genome. We used Bowtie 2 to align hpDNAs to the human reference genome (human_g1k_v37). The results are shown in Table S5.

SARS-CoV-2 assay

On day 1, cells were seeded into 24-well plates (Corning) at a density of 70 000 cells per well. On day 2, cells were transfected with pcDNA3.1(+)-HA -*A. fulgidus* FEN1-NES (1 μg per well). Vero cells were transfected 48 h prior to infection, cells were inoculated at MOI 0.008 and MOI 0.16 with SARS-CoV-2. After 1 h of inoculation, the inoculum was removed. Twenty-four hours later, cells were transfected with a hpDNAs pool (800 pmoL per well) (the detailed sequences are shown in Table S1, same as Fig. 2C). Finally, the cellular supernatant was collected for absolute quantification PCR.

For the study of the mutation of SARS-CoV-2 targets, the vRNA was reverse transcription with the HiScript III 1st Strand cDNA Synthesis Kit (+gDNA wiper) (Vazyme, R312-01). The N fragment was PCR amplified. To reduce nonspecific PCR products, high-fidelity DNA polymerase was used. cDNA (50 ng) was added as a template in a 20 μl of PCR mixture. The PCR program was 98°C for 5 min, 35 cycles (98°C for 10 s, 60°C for 5 s and 72°C for 30 s) and 72°C for 10 min. The products were purified using EasyPure PCR Purification Kit (TransGen, EP101-01, Beijing, China) following the manufacturer's protocol and analysed on 1% agarose gels. Gels were stained with GelRed stain and imaged. For Sanger sequencing analysis, PCR products corresponding to genomic modifications were purified and cloned with the *pEASY*®-Blunt Zero Cloning Kit (TransGen, CB501-01). Then, transformants for each group were randomly selected and sequenced to identify mutations using the M13 primer.

Absolute quantification PCR

To determine the quantity of SARS-CoV-2 in Vero cells, we measured viral RNA levels in the supernatant of infected cell cultures. Cell culture supernatants were processed by heat inactivation (95°C for 10 min). RT-qPCR was performed using the HiScript II One Step qRT-PCR Probe Kit (Vazyme Q222-01) according to the manufacturer's instructions. A standard curve of CoV-N fragment plasmid from 10^7 to 10 copies per microlitre was used to quantify the number of copies of viral RNA in each replicate. The average of each sample's three technical replicates was calculated. The sequences of primers and TaqMan probes are shown in Table S4.

The HBV cccDNA extraction and analysis

Cell pellets were collected and DNA was extracted using the Genomic DNA Kit (TransGen, EE101-01). DNA was extracted according to the manufacturer's protocol, and the final product was eluted in 30 μl of water. For cccDNA extraction and analysis, DNA extracted from cells was subjected to ON digestion with a plasmid-safe DNase (E3101K; Epicentre, Madsion, WI, USA). Following enzyme inactivation at 65°C for 10 min, DNA was subjected to HiScript II One Step qRT-PCR Probe Kit (Vazyme Q222-01) according to the manufacturer's instructions and using cccDNA specific primers (the detailed sequences are shown in Table S4). For quantification, a standard curve derived from decreasing concentrations of standard plasmid was used. PCR was performed using ABI 7500 Real-Time PCR System. Due to operational errors in cell counting and aspirating liquid in this experiment, there is a certain error in the quantification of the number of cccDNA per million cells. During the quantification of cccDNA, there is a certain error for the number of cccDNA per million cells. The experimental results mainly reflect the editing efficiency of AntiV-SGN.

The integrated HBV DNA extraction and analysis

Cell pellets were collected and DNA was extracted using the Genomic DNA Kit (TransGen, EE101-01). DNA was extracted according to the manufacturer's protocol, and the final product was eluted in 30 μl of water. And then, the integrated HBV DNA was isolated from genomic DNA by gel chromatography. DNA was subjected to relative quantitative PCR. The detailed sequences are shown in Table S4. And then, we testified whether the cccDNA was removed from the genomics of HepG2.2.15 cells completely. Genomic DNA extracted from cells and the integrated HBV DNA were subjected to ON digestion with a plasmid-safe DNase (E3101K, Epicentre).

Following enzyme inactivation at 65°C for 10 min, amplified the linearized genome using phi29 DNA polymerase (EP0091; Thermo Scientific™, Waltham, MA, USA) (the detailed primer sequences are shown in Table S4). And then, the alpha1 antitrypsin (A1AT) genomic DNA sequence and HBV S-ORF were amplified using specific primers (the detailed sequences are shown in Table S4). The results are analysed by 1% agarose gel electrophoresis.

Animal studies

The male C57/BL6 mice (6-week old, weighing 16–20 g) (Beijing HFK Bioscience Co., Ltd, Beijing, China) were injected with a mixture of 20 μg 1.3 × HBV plasmid, 40 μg FEN1-expressing plasmid or EV control plasmid, and 2200 pmoL targeting hpDNAs or non-targeting hpDNAs by the hydrodynamic injection (HDI) technique. Plasmids and hpDNAs were dissolved in 0.9% salt saline in a volume corresponding to 0.1 times the animal weight (in grams) and the mixture was injected through the tail vein in 5–8 s. After injection, the animals were sacrificed at the indicated time points to detect the HBV surface antigen (HBsAg) in peripheral blood and HBV fragment mRNA in the liver.

HBsAg ELISA

The HBsAg ELISA was performed using the HBsAg chemiluminescence Immunoassay kit (mlbio Human HBsAg ELISA KIT Cat. #SU-B11678) according to the manufacturer's instructions. Plates were read using the Varioskan Flash (Thermo Scientific).

IHC

The heart, spleen, lung and kidney of each group of C57/BL6 mice were fixed with 10% formalin, embedded in paraffin, deparaffinized and stained with haematoxylin–eosin staining solution. Observe the pathological changes of the organs under an optical microscope. This experiment uses paraffin sections of tissues. The sample slices were placed in an oven at 60°C for about 1 h until the sliced paraffin wax was in the shape of drops. Then, put it in xylene to dewax for 10 min, replace with new xylene and dewax again for 10 min. Soak the sample slices in absolute ethanol for 5 min, 90% ethanol for 2 min, 70% ethanol for 2 min and distilled water for 2 min. Then, the sample section was stained with haematoxylin staining solution for 10 min and washed with PBS for 10 min to wash away the excess staining solution. Wash with distilled water for 10 min, 95% ethanol for 5 s and stain with eosin staining solution for 30 s. Then, the sample slices were dehydrated in 95% ethanol for 2 min, replaced with 95% ethanol and dehydrated again for 2 min. Soak the sample slices in xylene for 5 min. Replace with xylene, soak again for 5 min, mount the tablet and observe under the microscope.

Statistical analysis

All data were expressed as mean ± SEM from two to four independent experiments performed in a parallel manner. Comparisons between two groups were analysed using two-tailed Student's *t*-tests. *P* values <0.05 were considered statistically significant.

Acknowledgements

The authors appreciate Yuan Gao, who works in the Pharmaceutical Animal Experimental Center of China Pharmaceutical University, for his kind help with *in vivo* experiments.

The authors would also like to thank Professor Jun Liao (China Pharmaceutical University) for the verification in the specificity of probes in the manuscript.

Conflict of interest

The authors declare that they have no competing financial interests.

Data availability statement

All data generated or analysed during this study are included in this article and its supplementary information files. The plasmids used in this study can be obtained from the corresponding authors upon request.

References

Abbott, T.R., Dhamdhere, G., Liu, Y., Lin, X., Goudy, L., Zeng, L., *et al*. (2020) Development of CRISPR as an antiviral strategy to combat SARS-CoV-2 and influenza. *Cell* **181:** 865–876.e812.

Abudayyeh, O.O., Gootenberg, J.S., Essletzbichler, P., Han, S., Joung, J., Belanto, J.J., *et al*. (2017) RNA targeting with CRISPR-Cas13. *Nature* **550:** 280–284.

Bella, R., Kaminski, R., Mancuso, P., Young, W.B., Chen, C., Sariyer, R., *et al*. (2018) Removal of HIV DNA by CRISPR from patient blood engrafts in humanized mice. *Mol Ther-Nucl Acids* **12:** 275–282.

Blanchard, E.L., Vanover, D., Bawage, S.S., Tiwari, P.M., Rotolo, L., Beyersdorf, J., *et al*. (2021) Treatment of influenza and SARS-CoV-2 infections via mRNA-encoded Cas13a in rodents. *Nat Biotechnol* **39:** 717–726.

Block, T.M., Guo, H., and Guo, J.T. (2007) Molecular virology of hepatitis B virus for clinicians. *Clin Liver Dis* **11:** 685–706.

Carrat, F., and Flahault, A. (2007) Influenza vaccine: the challenge of antigenic drift. *Vaccine* **25:** 6852–6862.

Chan, J.F., Kok, K.H., Zhu, Z., Chu, H., To, K.K., Yuan, S., and Yuen, K.Y. (2020) Genomic characterization of the 2019 novel human-pathogenic coronavirus isolated from a patient with atypical pneumonia after visiting Wuhan. *Emerg Microb Infect* **9:** 221–236.

Cox, D.B.T., Gootenberg, J.S., Abudayyeh, O.O., Franklin, B., Kellner, M.J., Joung, J., and Zhang, F. (2017) RNA editing with CRISPR-Cas13. *Science* **358:** 1019–1027.

De Clercq, E., and Li, G. (2016) Approved antiviral drugs over the past 50 years. *Clin Microbiol Rev* **29:** 695–747.

Freije, C.A., and Sabeti, P.C. (2021) Detect and destroy: CRISPR-based technologies for the response against viruses. *Cell Host Microbe* **29:** 689–703.

Ganem, D., and Prince, A.M. (2004) Hepatitis B virus infection--natural history and clinical consequences. *N Engl J Med* **350:** 1118–1129.

Hartenian, E., Nandakumar, D., Lari, A., Ly, M., Tucker, J.M., and Glaunsinger, B.A. (2020) The molecular virology of coronaviruses. *J Biol Chem* **295:** 12910–12934.

Hu, J.H., Miller, S.M., Geurts, M.H., Tang, W., Chen, L., Sun, N., *et al*. (2018) Evolved Cas9 variants with broad PAM compatibility and high DNA specificity. *Nature* **556:** 57–63.

Huang, C., Wang, Y., Li, X., Ren, L., Zhao, J., Hu, Y., *et al*. (2020) Clinical features of patients infected with 2019 novel coronavirus in Wuhan, China. *Lancet* **395:** 497–506.

Li, H., Sheng, C.Y., Liu, H.B., Liu, G.Z., Du, X.Y., Du, J., *et al*. (2016) An effective molecular target site in hepatitis B virus S gene for cas9 cleavage and mutational inactivation. *Int J Biol Sci* **12:** 1104–1113.

Loomis, K.H., Lindsay, K.E., Zurla, C., Bhosle, S.M., Vanover, D.A., Blanchard, E.L., *et al*. (2018) In vitro transcribed mRNA vaccines with programmable stimulation of innate immunity. *Bioconjug Chem* **29:** 3072–3083.

Margolis, D.M., Archin, N.M., Cohen, M.S., Eron, J.J., Ferrari, G., Garcia, V., *et al*. (2020) Curing HIV: seeking to target and clear persistent infection. *Cell* **181:** 189–206.

Price, A.A., Sampson, T.R., Ratner, H.K., Grakoui, A., and Weiss, D.S. (2015) Cas9-mediated targeting of viral RNA in eukaryotic cells. *Proc Natl Acad Sci U S A* **112:** 6164–6169.

Ramanan, V., Shlomai, A., Cox, D.B., Schwartz, R.E., Michailidis, E., Bhatta, A., *et al*. (2015) CRISPR/Cas9 cleavage of viral DNA efficiently suppresses hepatitis B virus. *Sci Rep* **5:** 10833.

Roehm, P.C., Shekarabi, M., Wollebo, H.S., Bellizzi, A., He, L.F., Salkind, J., and Khalili, K. (2016) Inhibition of HSV-1 replication by gene editing strategy. *Sci Rep* **6:** 23146.

Rojek, A., Horby, P., and Dunning, J. (2017) Insights from clinical research completed during the west Africa Ebola virus disease epidemic. *Lancet Infect Dis* **17:** E280–E292.

Sells, M.A., Chen, M.L., and Acs, G. (1987) Production of hepatitis B virus particles in Hep G2 cells transfected with cloned hepatitis B virus DNA. *Proc Natl Acad Sci U S A* **84:** 1005–1009.

Snijder, E.J., Limpens, R., de Wilde, A.H., de Jong, A.W.M., Zevenhoven-Dobbe, J.C., Maier, H.J., *et al*. (2020) A unifying structural and functional model of the coronavirus replication organelle: tracking down RNA synthesis. *PLoS Biol* **18:** e3000715.

Staahl, B.T., Benekareddy, M., Coulon-Bainier, C., Banfal, A.A., Floor, S.N., Sabo, J.K., *et al*. (2017) Efficient genome editing in the mouse brain by local delivery of engineered Cas9 ribonucleoprotein complexes. *Nat Biotechnol* **35:** 431–434.

Tian, K., Guo, Y., Zou, B., Wang, L., Zhang, Y., Qi, Z., *et al*. (2020) DNA and RNA editing without sequence limitation using the flap endonuclease 1 guided by hairpin DNA probes. *Nucleic Acids Res* **48:** e117.

Tiwari, P.M., Vanover, D., Lindsay, K.E., Bawage, S.S., Kirschman, J.L., Bhosle, S., *et al*. (2018) Engineered mRNA-expressed antibodies prevent respiratory syncytial virus infection. *Nat Commun* **9:** 3999.

V'Kovski, P., Kratzel, A., Steiner, S., Stalder, H., and Thiel, V. (2021) Coronavirus biology and replication: implications for SARS-CoV-2. *Nat Rev Microbiol* **19:** 155–170.

Wang, J., Li, J., Zhao, H., Sheng, G., Wang, M., Yin, M., and Wang, Y. (2015) Structural and mechanistic basis of PAM-dependent spacer acquisition in CRISPR-Cas systems. *Cell* **163:** 840–853.

Wolff, G., Limpens, R., Zevenhoven-Dobbe, J.C., Laugks, U., Zheng, S., de Jong, A.W.M., *et al*. (2020) A molecular pore spans the double membrane of the coronavirus replication organelle. *Science* **369:** 1395–1398.

Xu, C.F., Chen, G.J., Luo, Y.L., Zhang, Y., Zhao, G., Lu, Z.D., *et al*. (2021) Rational designs of in vivo CRISPR-Cas delivery systems. *Adv Drug Deliv Rev* **168:** 3–29.

Zhang, L.G., Richards, A., Barrasa, M.I., Hughes, S.H., Young, R.A., and Jaenisch, R. (2021) Reverse-transcribed SARS-CoV-2 RNA can integrate into the genome of cultured human cells and can be expressed in patient-derived tissues. *Proc Natl Acad Sci USA* **118:** e2105968118.

Supporting information

Additional supporting information may be found online in the Supporting Information section at the end of the article.

Fig. S1. The CoV-RdRP fragment mRNA relative expression of groups transfected with non-targeting hpDNA (NT) and targeting hpDNAs (Hp-R1, Hp-R2, Hp-R3, and Hp-R4). $n = 3$, two-tailed Student *t*-test; *P* values for Hp-R1 ($P = 0.0388$), Hp-R2 ($P = 0.0125$), Hp-R3 ($P = 0.0138$) and Hp-R4 ($P = 0.5409$) are relative to NT.

Fig. S2. HEK293T, HepG2 and A549 were treated by AntiV-SGN and CRISPR-Cas, and the cells viability inhibition was determined by CCK8 assay. $n = 4$ or 5.

Fig. S3. Specific PCR showing that HBV cccDNA can be removed totally by method of gel chromatography.

Table S1. All probe sequences used in the study, including hpDNAs, were tested for targeting CoV-N/HBV-X/CoV-RdRP reporters plasmids, SARS-CoV-2, HBV DNA, animal studies and non-targeting (NT) hpDNAs.

Table S2. The sequences of CoV-N/HBV-X/CoV-RdRP Reporter plasmids in the study.

Table S3. Spacer sequences (DNA) of crRNAs and sequences of siRNAs targeting CoV-N/HBV-X reporters plasmids in the study.

